

Partial photoionization cross sections of N₂ and CO using synchrotron radiation*

E. W. Plummer and T. Gustafsson

Department of Physics and Laboratory for Research on the Structure of Matter,[†] University of Pennsylvania, Philadelphia, Pennsylvania 19104

W. Gudat[‡] and D. E. Eastman

I.B.M. Thomas J. Watson Research Center, Yorktown Heights, New York 10598

(Received 17 November 1976)

The photon energy dependence of the partial photoionization cross sections and branching ratios for CO and N₂ have been measured using the continuum radiation produced by an electron storage ring. These measurements were conducted over the photon energy range of 14 to 50 eV. The partial photoionization cross sections in the energy region of the photoionization continuum are in good agreement with recent calculations where both the theory and experiment exhibit scattering resonances for specific states of the ion. The continuously variable photon energy source was utilized to examine the effect of autoionization on the partial photoionization cross section, showing in several cases quite different structure depending upon the final state of the ion.

I. INTRODUCTION

Photoelectron spectroscopy has proven to be a very useful method for studying the electronic states of atoms, molecules, solids, and solid surfaces. The most common measurement records the kinetic energies of the photoemitted electron from the atomic, molecular or solid states, or equivalently the various energies of the ionic states of the system. A much less common measurement is the relative intensity of each energy group as a function of the exciting photon energy. This partitioning of excited electrons amongst the various available excitation modes (ionic states of the system) in the process of photoionization is known as the branching ratio. If the absolute photoionization cross section is known or measured the values of the branching ratio can be used to give absolute values of the partial photoionization cross section.¹

Our interest in the photon energy dependence of the partial photoionization cross sections of simple molecules originates from photoelectron measurements of molecules adsorbed on surfaces.² One of the major objectives of photoelectron spectroscopy applied to surfaces is to identify the chemical nature of an adsorbed molecule. The simplest approach is to compare the electronic binding energies of an unknown molecule on the surface with likely candidates in the gas phase. This comparison is complicated, even for very weakly bound surface complexes, by the shift to higher kinetic energy of the photoemitted electrons caused by the relaxation of electrons of the substrate around the hole created by photoionization. This shift in the kinetic energy of the spectrum from an adsorbed molecule need not be a

rigid shift since it depends upon the detailed character of the orbit from which the electron is being removed.³ Nevertheless, a comparison of the relative spacings and intensities of the orbitals has proven to be a very useful technique to identify the chemisorbed molecule.^{4,5} The partial photoionization cross section can play a very important role in identifying energy levels of adsorbed molecules, especially the photon energy dependence of these cross sections. We have already demonstrated the power of this technique for surface studies, identifying the energy levels of molecularly adsorbed CO on Ni and Pd by their energy dependent cross sections.²

Our motivation for measuring the partial photoionization cross sections of the simple gas-phase molecules⁶ was twofold: (1) to catalog these partial cross sections for use in identifying chemisorbed molecules; and (2) to obtain in conjunction with theoretical calculations⁷ a more basic understanding of the photoionization process in the far ultraviolet wavelength region. A general objective is to predict the angular dependent emission for each ionic state for a molecule with fixed orientation, and then use this knowledge to determine the bonding geometry when this molecule is adsorbed on the surface of a single crystal. Obviously the angular dependence observed in the gas phase for random orientation⁸ will not be as pronounced as the angular effects for a molecule with its orientation fixed by the surface.

II. EXPERIMENTAL

All of the photoemission results reported in this paper were obtained at the 240-MeV storage ring at the Physical Sciences Laboratory of the

University of Wisconsin,⁹ using a system very similar to that previously described.¹⁰ In these experiments a 1-m Seya-Namioka-type monochromator was used to disperse the radiation from the storage ring. The usable range of this monochromator coupled to the storage ring was 10–50-eV photon energy. A plot of the photon flux out of the monochromator is given in the Appendix.¹¹ The light is predominantly polarized in the plane of the storage ring, even after being dispersed by the horizontally mounted monochromator.¹² The wavelength resolution of the monochromator is externally variable in steps from 1.6 to 16 Å FWHM. The experimental chamber is pumped with an ion pump as are the monochromator and the beam line. The pressure differential over the slits of the monochromator effectively isolates the ultrahigh vacuum in the storage ring from the experiment.

The photoemitted electrons are energy analyzed by a double-pass cylindrical mirror analyzer (CMA),¹³ whose axis is perpendicular to both the direction and polarization of the light (within 5°). This geometry consequently integrates over a fairly large set of polar angles. The analyzer is operated in constant pass energy mode, where an energy distribution is obtained by accelerating or retarding the electrons between two concentric hemispherical grids. The two apertures in the analyzer corresponded to an effective aperture of 1.2 mm in diameter. The pass energy was adjustable. Except at low pass energies (≤ 15 eV), the resolution of the energy analyzer is $\Delta E/E \approx 0.8\%$.

The gas enters the system through a 1-mm capillary tube approximately 25-cm-long concentric with the analyzer axis. During operation the background pressure in the vacuum chamber was maintained at approximately 5×10^{-6} Torr, while the estimated pressure right above the nozzle was $\sim 10^{-4}$ Torr.¹⁴ Both the light beam and the gas beam were approximately 1 mm in diameter at the focal point of the analyzer. Therefore the major region of interaction was a volume of approximately 1 mm³. This small volume enabled the energy analyzer to be operated in a mode where the acceptance volume exceeded the volume of excitation. This was achieved by accelerating the electrons into the analyzer and operating at a pass energy which exceeded the maximum kinetic energy of the photoemitted electrons. This operational mode results in relatively poor resolution (~ 0.3 – 0.4 eV) but has the distinct advantage that the collection efficiency of the analyzer is independent of energy. The best resolution obtained so far is ~ 0.17 eV, allowing us to resolve, e.g., the vibrational levels in CO and N₂. The Appendix

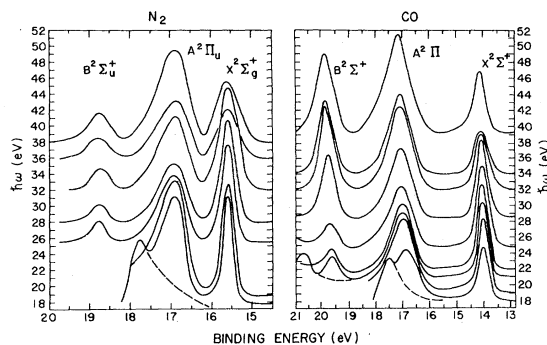


FIG. 1. Photoemission energy distributions for CO and N₂ at selected photon energies $\hbar\omega$. The emitted intensity is plotted as a function of binding energy. The numbering of the vertical scale refers to the photon energy at which the distribution was obtained. The curves are hence displaced relative to each other with amounts proportional to the differences in photon energy. The pass energy of the analyzer was 40 eV for the CO data and 33 eV for the N₂ data. The dashed lines represent the background.

gives a more detailed description of measurement techniques and the measured transmission of this system.

Figure 1 shows electron energy distributions for CO and N₂ at several photon energies. The energy distributions are plotted as a function of binding energy which is the photon energy minus the kinetic energy.

As discussed in the Appendix, we wish to use the energy analyzer with a high pass energy. This has the additional advantage that the counting rates are increased. The highest value of analyzer pass energy used was determined by the resolution limits imposed by the photoelectron spectra. For example, the CO spectra were accumulated with a higher pass energy than the N₂ spectra because the peaks are more separated in energy. The majority of the spectra were accumulated in a multichannel analyzer sweeping in an up-down mode to average out drifts in the gas pressure and photon flux.

The number of photoemitted electrons detected for a given ionic state i not only depends upon the partial photoionization cross section σ_i but upon the angle of collection θ ,⁸ with respect to the direction of polarization. The measured signal I is proportional to¹⁵

$$I \propto \frac{\sigma_i}{4\pi} \int_{\Omega} [1 + (\beta_i/2)(3 \cos^2 \theta - 1)] d\Omega,$$

where the asymmetry parameter β_i characterizes the angular distribution from the i th ionic state at a given photon energy.¹⁵ Ω is the solid angle accepted by the analyzer. For the geometry of

this experiment

$$I_i \propto \sigma_i [1 - 0.16\beta_i] \quad (1)$$

assuming 100% polarization of the light perpendicular to the axis of the analyzer.

The basic measurements in this paper are the branching ratios. These are obtained by recording an energy distribution at a fixed photon energy, like those shown in Fig. 1, and then measuring the area under each peak. A smooth background was subtracted from the low-energy part of each curve, shown by the dashed lines in Fig. 1, and the areas under each of the peaks measured. The background was caused by ions or light from the ion pump and synchrotron light striking the magnetic shielding around the analyzer. We measure a branching ratio B_m^i , given by

$$B_m^i = A_i / \sum A_i,$$

where A_i is the area of the i peak and the sum is over all observed states of the ion. Since our analyzer has a constant collection efficiency (see Appendix)

$$I_i = cA_i, \quad (2)$$

where c is independent of i . The actual angle-integrated branching ratio for the i th level B^i is defined as

$$B^i = \sigma_i / \sum \sigma_i,$$

where the sum is over all possible states of the ion which are energetically allowed.

When $\beta = 0$, i.e., an isotropic source, our measured branching ratios B_m^i would be equal to the actual values B^i . For all other values of β_i we have

$$B_m^i = \frac{B^i(1 - 0.16\beta_i)}{\sum_j B^j(1 - 0.16\beta_j)}. \quad (3)$$

The measured values of B^{i1} and β_i ⁸ for CO at $\hbar\omega = 21.2$ eV are $8.7 \pm 0.4\%$ and 1.0 ± 0.2 for the $B^2\Sigma^+$ state; $57.4 \pm 1.4\%$ and 0.3 ± 0.1 for the $A^2\Pi$ state and $33.9 \pm 1.4\%$ and 0.8 ± 0.1 for the $X^2\Sigma^+$ state, respectively. Inserting these values in Eq. (3) would give calculated B_m 's of $8.0 \pm 1.1\%$ for the $B^2\Sigma^+$ state, $59.7 \pm 5.5\%$ for the $A^2\Pi$ state and $32.3 \pm 3.6\%$ for the $X^2\Sigma^+$ state with our experimental geometry. Ignoring the errors in the measured values^{1,8} this gives a geometry-dependent error of 8, 4, and 4.7%, respectively, for the three levels as measured with our geometry. Our measured values at this photon energy are 11.5, 58.5, and 30.0%, respectively, which lie within the error of the calculated values with the exception of the

$B^2\Sigma^+$ state. Our data are hence consistent with what has been measured at $\hbar\omega = 21.2$ eV. We conclude that the geometry of our measurement will not result in serious errors for the branching ratios.

The photoionization cross section and, consequently, the partial photoionization cross section will exhibit sharp structure due to autoionization near the ionization threshold. These rapid variations with photon energy are difficult to follow using the above-mentioned technique of integrating areas in energy distributions. The continuum characteristics of synchrotron radiation can be utilized in a mode in which the photon energy is swept while fixing the ionic state which is being observed. This mode of operation which is referred to as "constant initial-state-energy spectra" (CIS's) has been used to map out final-state (kinetic energy) effects in solids.¹⁶ The principle is quite simple: The transmitted kinetic energy of the electron energy analyzer is swept synchronously with the photon energy, so that $\hbar\omega - E_{ke}$ is a constant. The kinetic energy of a photoejected electron from a molecule is given by

$$E_{ke} = \hbar\omega + E_0 - E_{ion}^i$$

where E_0 and E_{ion}^i are the total energies of the neutral molecule and ion, with the ion in the i th state and the neutral molecule in the ground state. In the CIS mode we therefore look at photoionization into a specific ionic configuration. For example, if $\hbar\omega - E_{ke} = 15.7$ eV for N₂ the ionic state is $X^2\Sigma_g^+$. This indicates that the acronym CIS might be interpreted as "constant ionic state." One strength of the CIS technique is obviously that it allows us to separate overlapping bands in the photoabsorption spectrum.

In molecular CIS photoemission measurements, the signal recorded for a given value of $\hbar\omega - E_{ke}$, (i.e., for a particular ionic state) is proportional to the partial photoionization cross section,¹⁷ the gas pressure, the light intensity, the transmission of the energy analyzer, and the volume of intersection of the gas and light beams. Only the cross section, light intensity and analyzer transmission depend upon photon energy. As stated above, the analyzer was usually operated at high pass energy to remove the energy dependence. The effect of the large variation of the photon flux with photon energy (see Appendix) was approximately included by dividing the signal out of the electron energy analyzer by the photocurrent from a gold foil.¹⁸ This gold foil was positioned next to the exit slits of the monochromator and subtended 12 Å of the dispersed light. If the photoyield of the gold foil was independent of photon energy then the signal would be proportional to the

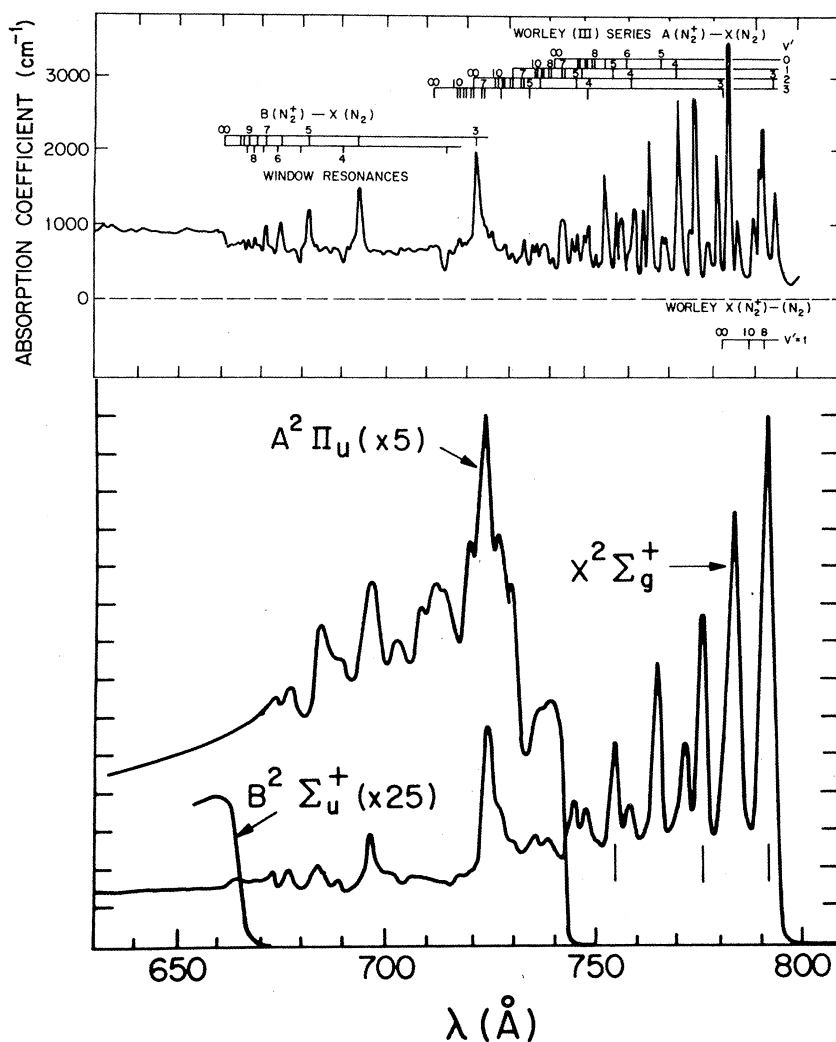


FIG. 2. CIS (constant ionic state) curves for the $X^2\Sigma_g^+$, $A^2\Pi_u$, and $B^2\Sigma_u^+$ ionic states of N_2 as a function of the wavelength of the incident light. The values of $\hbar\omega - E_{ke}$ used correspond to the measured binding energies. The energy analyzer pass energy was 40 eV. The top curves are the absorption spectrum for N_2 , reproduced from Huffman *et al.* (Ref. 53) ($\Delta\lambda = 0.5 \text{ \AA}$). There are some slight differences in the energy location of structure between Ref. 53 and the present work. We believe these to be instrumental in origin.

partial-photoionization cross section.¹⁹ Figure 2 shows (on the bottom) our CIS spectra for three ionic states of N_2 plotted vs wavelength. The wavelength resolution of the monochromator was 1.6 \AA and the electron-energy analyzer pass energy was 40 eV. It is obvious from Fig. 2 that this mode is a very convenient way to obtain the position and relative intensity of the fine structure in the partial-photoionization cross section near the ionization threshold. We stress that the curves shown in Fig. 2 (and in Fig. 7) are proportional to the photoionization cross section *times the inverse of the photoyield of the Au foil.*

III. RESULTS

Each peak in the kinetic-energy distribution of photoemitted electrons represents a different state or states of the ion, as given by Eq. (4). The electrons with the largest kinetic energy represent the ground states of the ion, while all other peaks

correspond to excited states of the ion. It is convenient, but in some cases confusing, to separate the excited states of the ion into two categories: (1) those which can be identified with a one-electron excitation, and (2) all others, presumably due to multielectron excitations. We will discuss the following data in this fashion. The first section will describe the branching ratios and partial cross sections, concentrating on the region of the ionization continuum. The second section will describe the CIS measurements and discuss the effects of autoionization. The final section will, where appropriate, discuss our observations of multielectron excitations.

A. CO

1. Energy distributions, branching ratios, and partial cross sections

The measured branching ratios for the four lowest-lying one-electron states and three multi-

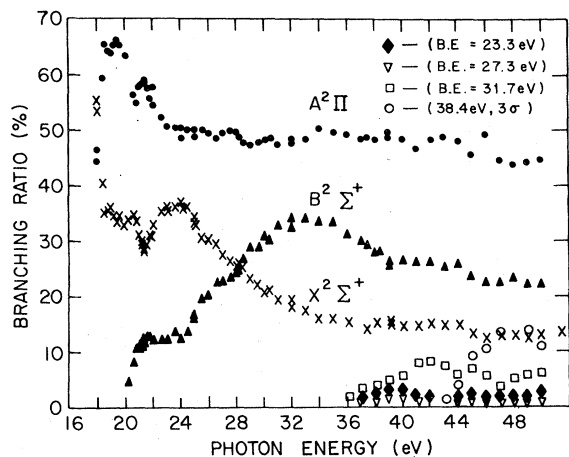


FIG. 3. Measured branching ratios for the four lowest energy ionic states of CO as a function of photon energy. Three multielectron excited states are also shown and indicated solely by their binding energies.

electron states of CO⁺ are shown in Fig. 3. This plot covers the photon-energy range of 18–50 eV. Below 18 eV there are too many rapid oscillations in the branching ratios, due to autoionization, to be followed by this method. This region will be discussed in the next section. Above 50 eV the photon flux was too low to make measurements in a reasonable time (< 1 h/photon energy).

The partial-photoionization cross sections¹⁷ were calculated from the data shown in Fig. 3 and the total absorption cross sections obtained by Lee *et al.*²⁰ The photoionization yield was taken to be one since Samson and Gardner's data¹ indicate that it is > 0.95 for $\hbar\omega > 18$ eV, and the electron-energy-loss electron-ion coincidence work of Wight *et al.*²¹ shows an ionization efficiency of one above ~19 eV. The partial photoionization cross sections obtained in this manner are shown in Fig. 4.

Before we discuss the features of Fig. 4 which are due to photoionization into the continuum, we must discuss briefly the structure between 19 and 22 eV in the A²Π and X²Σ⁺ ionic states, which is believed to be partially due to autoionization. Both Codling and Potts²² and Sasanuma *et al.*²³ have observed structure in the absorption spectra of CO between 20 and 23 eV. The absorption spectra of Sasanuma *et al.*²³ reveals a broad minimum at 21.4 eV with a 4 or 5% decrease in the absorption cross section. Since we used the data by Lee *et al.*²⁰ which show a nearly constant-absorption cross section in this photon-energy region, the possible decrease in the absorption cross section at 21.4 eV^{22, 23} might remove part of the structure in the A²Π state at 21.4 eV (in Fig. 4). It would also accentuate the minimum in the X²Σ⁺ state at 21.4 eV. We believe that the dip in the X²Σ⁺ state cross section at 21.4 eV and the peak at ~23 eV

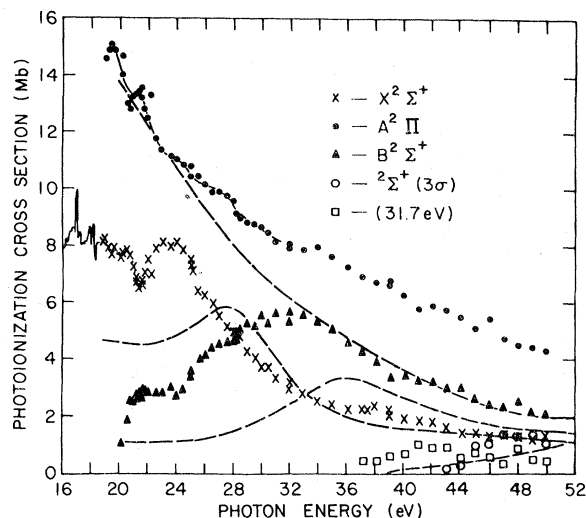


FIG. 4. Partial photoionization cross sections (Ref. 17) for the four lowest energy one-electron ionic states of CO as well as one multielectron excited state as a function of photon energy. The solid curves have been obtained from CIS spectra. The dashed lines are the results of Davenport's calculation (Refs. 7 and 25).

are not primarily the result of autoionization, while the rise below 21.4 eV is probably a consequence of autoionization.

The four one-electron excitation states of the CO ion shown in Figs. 3 and 4 are labeled X²Σ⁺, A²Π, B²Σ⁺, and ²Σ⁺(3σ). They correspond to removal of one electron from the 5σ, 1π, 4σ, and 3σ molecular orbitals of CO, respectively. The observed vertical ionization potentials are 14, 17, 19.7, and 38.3 eV. All three of the Σ states exhibit peaks in their cross sections due to scattering resonances in the *final* state, at approximately 10-eV kinetic energy (see Fig. 4). We have listed the kinetic energies of these resonances as well as their widths in Table I. This shape resonance was first discussed by Dehmer and Dill²⁴ for N₂ using a SCF-SW Xα calculation for the photoionization from the N 1s level. Davenport⁷ has used this method to calculate the photoionization cross sections for the valence levels of CO and N₂. His calculated results are shown by the dashed lines in Fig. 4.

The calculated partial photoionization cross sections agree qualitatively with the data and are in much better quantitative agreement than any previous calculation. The reproduce the general trends in each of the ionic states: The A²Π cross section decreases rapidly above threshold, while the Σ states have an increasing cross section just above threshold. There are shape resonances predicted in all three of the Σ states but not in the A²Π state,⁷ which agrees with our observations. The position of the resonances and their widths

TABLE I. Shape resonances in N₂ and CO.

Molecule	State	Peak position Kinetic energy (eV)		Resonance width (eV)	
		Experiment	Theory	Experiment	Theory
CO	X ² Σ ⁺	9.6	14 ^b	8	6.5 ^b
	B ² Σ ⁺	12.3	16.5 ^b	10	8 ^b
	² Σ ⁺ (3σ)	~11-12 ^c	16.7 ^b	~8-10	12 ^b
N ₂	1σ removed		11.3 ^a		3.7 ^a
			16.8 ^b		6.0 ^b
	X ² Σ _g ⁺	12.5	15.6 ^b	9	5.5 ^b

^aSCF- $X\alpha$ calculations by Dehmer and Dill (Ref. 24) using $\alpha = 1$.

^bSCF- $X\alpha$ calculations by Davenport (Ref. 7) using $\alpha_C = 0.75928$, $\alpha_N = 0.7510$, and $\alpha_O = 0.744470$.

^cSee Ref. 26.

do not agree exactly with the measurements as can be seen from Fig. 4 or Table I. The calculated kinetic energies are consistently too high. These resonances would undoubtedly be pulled down if the potential in the calculation was made more attractive, as it should be for the case of the ionic potential. For example, Davenport²⁵ has also calculated the position of the resonance energy using a transition-state potential. The resonances then occur at a lower kinetic energy than the experimental values. It is evident that the basic physics of the process is given by the existing calculations.^{7,24} This shape resonance occurs in the $l=3$ partial wave which has σ symmetry. In the photoionization spectra of N₂, which we will discuss in the next section, the resonance will not appear in the B²Σ_u⁺ state of N₂⁺ because a selection rule originating in the inversion symmetry, will not allow it.

Table I shows that the resonance does not occur at the same kinetic energy for each state of the ion. This is a result of the matrix elements coupling the different initial states to the continuum and shows the importance of the initial-state wave function. Experimentally we observe a 2.7-eV shift of the kinetic energy of the resonance for the B²Σ⁺ state relative to the X²Σ⁺ state. The theory gives 2.5 eV. The width of the resonances are also different for the two states, with an experimental ratio of 1.25 (B²Σ⁺ with respect to X²Σ⁺). The theoretical value is 1.23, which is very close to the experimental value.

According to Davenport's⁷ calculation, the shape resonance in the B²Σ⁺ state of CO⁺ is excited only by the component of the electric field which is parallel to the axis of the molecule, and the emission is in a narrow tube extending out of the oxygen end of the molecule. Recent angle resolved experiments with CO adsorbed on single-crystal Ni surfaces have shown that this resonance exists

at ~35-eV photon energy for p -polarized light and collection normal to the crystal,²⁷ but not for s polarized light. This could only occur if CO is terminally bonded to the nickel with the oxygen end sticking *straight* up. We mention this just to illustrate an obvious application of gas-phase photoionization work to surface physics.

2. Comparison with other measurements

In Fig. 5 our data for the branching ratios for CO⁺ (dashed lines) are compared with photoelectron-energy distribution measurements of Samson and Gardner,¹ Rabalais *et al.*²⁸ (for 90° collection angle relative to the propagation direction of the light), and Bahr *et al.*²⁹

The data of Samson and Gardner¹ were measured at an angle of 54.7° with respect to the direction

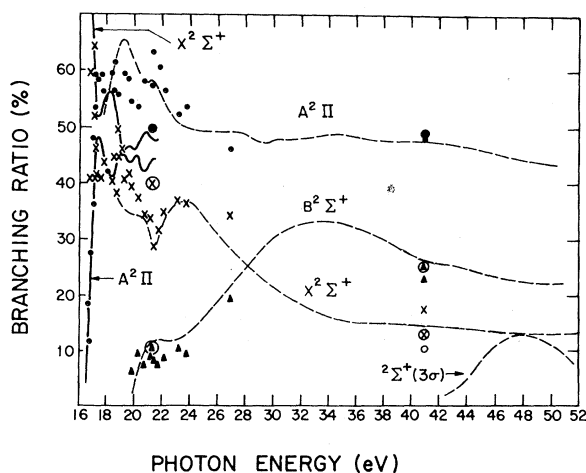


FIG. 5. Comparison of our branching ratio data (dashed lines) with other measured values. The \times 's, \bullet 's, \triangle 's, and \circ 's are for the X²Σ⁺, A²Π, B²Σ⁺, and ²Σ⁺(3σ) states from Samson and Gardner.¹ Circled points, Rabalais *et al.* (Ref. 28). Solid curves indicated at the left, Bahr *et al.* (Ref. 29).

of the light beam. There is then no dependence on β . Our data are in very good agreement with theirs. We pointed out in Sec. II that our value for the $B^2\Sigma^+$ state at 21.2 eV, when corrected for our geometry, is approximately 3% higher than Samson and Gardner's¹ but may fall within the error limits of the measurements. Both sets of measurements show the structure near 21.6 eV. At 40.8-eV photon energy our relative values for the first three states agree well with Samson and Gardner's,¹ but their value of 10.5% for the $^2\Sigma^+(3\sigma)$ state of the ion is much larger than we would estimate. We do not present any data for this state at $\hbar\omega = 40.8$ eV because of the serious difficulties in separating this state from the low energy scattered electrons. Our estimate from Fig. 4, using the general shape of a Σ state cross section is that the branching ratio for this state at 40.8-eV photon energy would be less than 3%. Our measured binding energy for the $^2\Sigma^+(3\sigma)$ state is 38.3 eV, while Gardner and Samson³⁰ report a value of 39.7 eV. Our value agrees very well with the value determined from ESCA,³¹ but is one volt higher than the value reported by Potts and Williams³² using filtered HeII radiation. These authors report a 3% value for the branching ratio of the $^2\Sigma^+(3\sigma)$ state at 40.8 eV. The reason for the large variation in measured binding energy for the state at $\hbar\omega = 40.8$ eV is that it is broad and hard to separate from the secondary electrons. Our value for the binding energy was determined from photoelectron energy distribution spectra at photon energies above 45 eV.

The data of Rabalais *et al.*²⁸ were taken at a 90° collection angle using unpolarized light, whereas our experimental setup integrates over a set of collection angles. We expect then a considerable deviation from our data due to different angular dependence of each orbit.⁸ If we, however, correct Rabalais *et al.*²⁸ data for the known β factors,⁸ the agreement is in fact worse than that shown in Fig. 5. At 40.8 eV we have plotted the data of Ref. 28 for the first three levels normalized to 90% to correspond to our percentage ratios for the deeper lying levels. The solid curves in Fig. 5 are from Bahr *et al.*²⁹ for the $X^2\Sigma^+$ and $A^2\Pi$ states of CO^+ . Their data seem to disagree with all other data in the ordering of the intensities of the outer two levels.

Figure 5 illustrates the limitations of conventional light sources for determining the photon-energy dependence of the partial photoionization cross section above ~ 24 eV. For example, one surely can not verify the existence of the resonance in the $B^2\Sigma^+$ state of CO^+ from the data of Ref. 1. Fortunately there is another type of experiment which is capable of measuring the

branching ratios as a function of energy. When high-energy electrons are inelastically scattered through very small forward scattering angles, they simulate photons of energy equal to the energy lost by the electron.³³ If both the high-energy electrons and the low-energy ejected electron beams are energy analyzed and measured in coincidence, then the branching ratios can be determined for any "photon energy." Brion and co-workers³³ have reported such electron-coincidence measurements for CO from 18 to 50 eV.

The data obtained for the branching ratios of CO from the electron impact, electron-coincidence measurements³³ are compared to our data in Fig. 6. We have used the same symbols for the various states as we did in Figs. 3–5. The data points contained within the circles are the results published in 1972, while the other data were published in 1976.³³ The 1972 results only reported the relative strength of the first three states of $\text{CO}^+(X^2\Sigma^+, A^2\Pi, \text{ and } B^2\Sigma^+)$, so we have scaled the branching ratios of these states for "photon energies" above 27 eV to account for the higher binding energy states reported in the 1976 data.³³ For clarity we do not plot the multielectron states (Fig. 3) in Fig. 6, but within experimental error our results agree with those of Hamnett, Stoll, and Brion.³³

In general the electron-coincidence results are in good agreement with our data. There are noticeable discrepancies, for example the structure in the $X^2\Sigma^+$ state from 21 to 25 eV does not seem to appear in the electron-coincidence data, and as a consequence the $A^2\Pi$ branching ratio appears to be too large. Both of these discrepancies may simply be caused by the fact that the resolution in the electron-coincidence work is

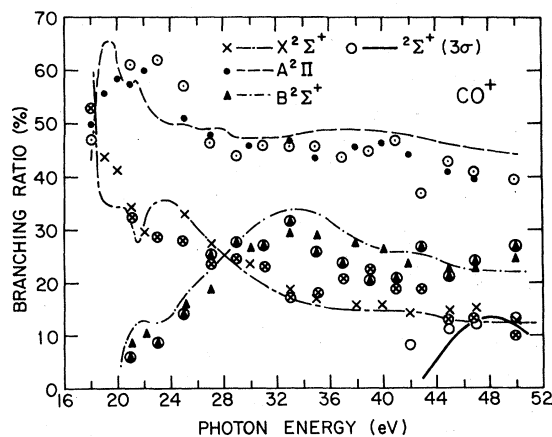


FIG. 6. Comparison of our branching ratio data for the one-electron states of CO^+ with the data obtained using the high-energy inelastic electron-coincidence technique (Ref. 33). The solid and dashed curves are reproduced from our data shown in Fig. 3.

worse than in the photoemission work.

Backx *et al.*³⁴ have used an electron triple-coincidence experiment, involving ions, electrons, and photons to determine the partial photoionization cross section of the $B^2\Sigma^+$ state of CO^+ . They normalized their data at 35 eV using absolute oscillation strengths measured by El-Sherbine and Van der Wiel³⁵ and the branching ratios shown in Fig. 6 measured by Van der Wiel and Brion.³³ The agreement between their data and ours shown in Fig. 4 is excellent. It would be even better if we used our branching ratios and the absorption cross-section data of Lee *et al.*²⁰ to normalize their data. The conclusion is that the electron-coincidence data offers independent verification of the existence of the resonance in the $B^2\Sigma^+$ state of CO^+ .

There is still another method which is used to obtain the partial photoionization cross sections of excited states of the ion. The intensity of the fluorescent decay into the ground state of the ion is measured as a function of the exciting photon energy. Lee *et al.*^{36,37} have reported the partial-photoionization cross sections for the $B^2\Sigma^+$ and $A^2\Pi$ states of CO^+ . The $A^2\Pi$ cross section has the same shape as our results (Fig. 4) but is uniformly lower in intensity.³⁶ Wight *et al.*²¹ have already pointed out that the fluorescent yield data for the $B^2\Sigma^+$ state are very different from the electron-coincidence data.^{33,34} It is also much different from our data in that it shows no sign of the resonance. However, very recent results by Lee^{37b} for the $B^2\Sigma^+$ state of CO^+ seem to agree much better with our data.

3. Autoionization of CO

Autoionization can be viewed in a simplistic way as a two step process: The molecule is first excited into a high-energy state of the neutral which exists for some time. Then it decays to a lower-energy ionic state emitting an electron via coupling to the continuum.^{38,39} The width of an autoionization peak is related to the life time of the intermediate excited bound state. The spectral shape is determined by the phase and relative amplitude of this process compared to direct photoionization into the continuum.³⁹ We have plotted the CIS curves for the three lowest-energy states of CO^+ in Fig. 7. In contrast to Fig. 2 these curves are plotted as a function of photon energy instead of wavelength. The structure in the $X^2\Sigma^+$ state is more complicated near threshold than the equivalent state for N_2 (see Fig. 2), presumably due to the increased number of transitions which are allowed due to the removal of symmetry selection rules.⁴⁰

Much of the structure below 17 eV has not been identified either in absorption⁴⁰ or ionization,⁴¹ consequently we have not tabulated these peaks in any detail. On the top of Fig. 7 are shown several of the Rydberg series converging to the $A^2\Pi$ state of CO^+ .⁴¹ The autoionization spectrum for energies above 17 eV is simpler and has been tabulated in Table II. Tanaka⁴² identified two Rydberg series called sharp and diffuse converging to the $B^2\Sigma^+$ state of CO^+ . These series are shown in Fig. 7 and tabulated in Table II. Ogawa⁴³ identified two other Rydberg series $R(\text{III})$ and $R(\text{V})$ (Table II)

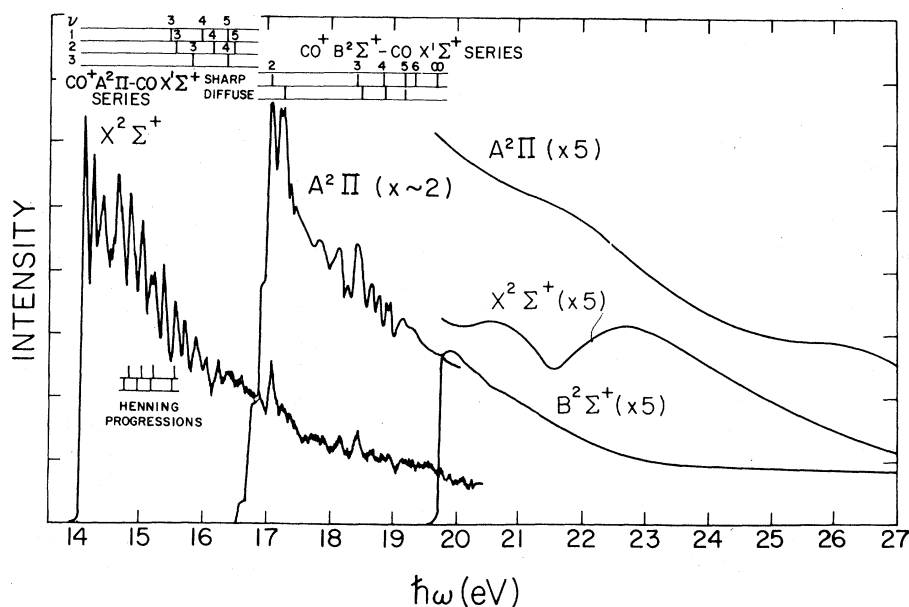


FIG. 7. CIS curves for three ionic states of CO^+ as a function of photon energy. The values of $\hbar\omega - E_{\text{ke}}$ used correspond to the measured binding energies. The analyzer pass energy was 40 eV and the slit width of the monochromator was 1.6 Å below 19.5 and 4 Å above that energy.

TABLE II. Prominent features in partial photoionization cross sections of CO beyond 17 eV.

λ (Å)	E (eV)	Tanaka	Assignment ^a	Ogawa
726	17.07	$R(S)m=2, v'=0$		
721	17.19			
717	17.28	$R(D)m=2, v'=0$		
691	17.93	P_4	$R(IV)m=3, v'=0$	
682	18.17	P_4	$R(IV)m=3, v'=1$	
679	18.27	Apparent emission series		
673	18.41	$R(S), R(D)m=3, v'=0$	$R(S)m=4, v'=0$	
665	18.63	$R(S), m=3, v'=1$	$R(S)m=4, v'=1$	
659	18.80	$R(S), m=3, v'=2$	$R(S)m=4, v'=2$	
			$R(III)m=5, v'=0$	
654	18.92	$R(S)m=4, v'=0$	$R(S)m=5, v'=0$	
			$R(IV)m=4, v'=0$	
650	19.06	Apparent emission series		
648	19.12	$R(S), R(D)m=4, v'=1$	$R(III)m=6, v'=0$	
			$R(S), R(D)m=3, v'=1$	

^a $R(S)$ and $R(D)$ refer to a sharp and diffuse Rydberg series converging to the $B^2\Sigma^+$ state of N_2^+ (Tanaka, Ref. 42), P 's are progressions (Ref. 40) and $R(N)$'s are new Rydberg series identified by Ogawa (Ref. 43). The m is the member of the series and v' is the vibrational state.

which also converge to this state of CO^+ . Ogawa⁴³ showed that Tanaka's⁴² numbering of the members of the sharp and diffuse series was displaced by one, so that the numbers shown in Fig. 7 should be increased by one. This is reasonable when you compare this Rydberg series with the equivalent series in N_2 . (See assignment in Fig. 2.) The third member of the N_2 series occurs at 17.14 eV which is 0.43 eV from the ionization threshold of the $A^2\Pi_u$ state of N_2^+ . The peak that Tanaka⁴² identified as the second member ($m=2$) of this Rydberg series in CO occurs at 17.07 eV which is 0.5 eV from the $A^2\Pi$ ionization threshold for CO. Therefore, these two peaks should belong to the same member of the series, i.e., $m=3$.

When the amplitude for autoionization and direct ionization into the continuum are comparable, the interference between the two processes can create very asymmetrical line shapes.³⁹ This interference can result in decreases in the cross section, sometimes called "window resonances." This effect is very pronounced in the Hopfield-Rydberg series converging to the $B^2\Sigma_u^+$ state of N_2^+ . For example there are noticeable dips in the absorption cross section of N_2 shown in Fig. 2 at 716 Å (17.3 eV) and at 690 Å (18 eV). These "window resonances" are not as pronounced in CO, but two were observed, one at 18.27 eV and the other at 19.06 eV. As in the case of N_2 they appear to be more pronounced in the cross section for the $A^2\Pi$ state of CO^+ than in the $X^2\Sigma^+$ state. It is also easy to see from Fig. 7 that the diffuse

members of the Rydberg series are more pronounced in the $A^2\Pi$ state than in the $X^2\Sigma^+$ state of CO^+ .

Several vibronic effects have been observed in our data. For example, the first autoionization peak (at $\hbar\omega \approx 14.1$ eV) in the $X^2\Sigma^+$ curve for CO^+ (Fig. 7) has been identified as the eighth member of a Rydberg series converging to the first vibrational state of the $X^2\Sigma^+$ state of CO^+ .⁴⁰ If this peak has been properly identified, then autoionization occurs through a vibronic coupling and *not* an electronic coupling. This effect will be discussed in Sec. III B 2. A second example of vibronic effects can be seen in the $A^2\Pi$ state curve of Fig. 7. The first few tenths of a volt above threshold in this state shows three distinct steps. We interpret these as the ionization thresholds of different vibrational levels of this state. If the background can be subtracted out one should be able to determine the partial cross sections of the vibrational states right at threshold with this method.

The resolution of the energy analyzer can be increased by decreasing the pass energy until each of the vibrational levels of the $X^2\Sigma^+$ state are resolved. With this resolution CIS curves could be recorded for each vibrational state of the $X^2\Sigma^+$ ionic state separately. In general these curves do not exhibit the striking effects that we have seen in NO and O_2 ,⁴⁴ but at $\hbar\omega = 15.55$ eV (797 Å) the cross section for the second vibrational state was considerably larger than for the first. This autoionization peak has been identified with a

Henning progression.⁴¹ The next members of the progression are at 15.36 eV (807 Å) and 15.23 eV (814 Å). The second vibrational-state cross section was also abnormally large for these two autoionization states.

The second vibrational state is also large near 17.2 eV (720 Å) which is the third member of the diffuse Rydberg series to the B state, while it is unaffected by autoionization from the corresponding sharp line. The fact that autoionization from the diffuse Rydberg series is larger than the sharp series in the $A^2\Pi$ cross section probably indicates that the potential energy for the Rydberg states corresponding to the diffuse series has its minimum at larger internuclear spacing than the sharp series.

Finally we return to the structure in the partial photoionization cross section between 20- and 22-eV photon energy which we briefly discussed previously. Codling and Potts²² have identified the fine structure in an absorption spectrum in this energy range as belonging to Rydberg series converging to ionic states of CO analogous to the $C^2\Sigma_u^+$ state of N_2 .⁴⁵ The intensity of this structure is very weak, being most intense around 20.5 eV. We believe that the peak in the $X^2\Sigma^+$ cross section at 20.5 eV is caused by autoionization from these states. How much of the dip in the cross section for this state at 21.6 eV is caused by interference effects is unclear. It is also possible that the variations in the $A^2\Pi$ cross section in this region can be caused by an interference effect creating a dip near 21 eV, or by the difference in coupling between these two ionic states and the various excited states of CO.²² The important feature is that autoionization in this energy region is much less pronounced in CO than in N_2 , as we will see below.

4. Multielectron excited states of CO

There have been several papers published reporting the observation with uv radiation of multielectron excited states of CO^+ with binding energies between the $B^2\Sigma^+$ state (19.7 eV) and the $^2\Sigma^+(3\sigma)$ (38.3 eV). Codling and Potts²² reported seeing a state with a (vertical) binding energy of ~23.5 eV in a 40.8-eV spectrum. Potts and Williams³² using a filtered HeII light source reported observing five such states with binding energies 22.7, 23.4, 25.3, 28.1, and 31.8 eV, the 31.8-eV state being the most intense. In contrast, Gardner and Samson³⁰ could not detect any of these excitations using HeII radiation dispersed by a monochromator. They suggested³⁰ that the different results were a consequence of using an uncalibrated analyzer with a filtered light source.

Our measurements were made with a dispersed

light source using an analyzer of known transmission. We observe three well separated peaks with binding energies between 20 and 38 eV; namely at 23.3, 27.3, and 31.7 eV. These peaks are, in comparison with the single-electron states, quite weak. Due to signal to noise problems our measurements do not exclude the existence of more, still weaker, multielectron states in this energy region. The branching ratios for these levels are shown in Fig. 3. The energy position and relative intensities for these levels at $\hbar\omega = 50$ eV agree quite well with the ESCA data at $\hbar\omega = 1254$ eV.³¹ At this photon energy the $B^2\Sigma^+$ state has a much larger cross section than either the $A^2\Pi$ or $X^2\Sigma^+$ states, five times larger than the $A^2\Pi$ and 2.5 times larger than the $X^2\Sigma^+$ state. Since the ratio of the intensity of the three multielectron states, with respect to the intensity of the $B^2\Sigma^+$ state, is almost the same at $\hbar\omega = 50$ eV (Fig. 3) as it is at $\hbar\omega = 1254$ eV,³¹ we suggest that these states are "shake up" states of the $B^2\Sigma^+$ state. Another piece of evidence which may support the conclusion is the fact that these states seem to exhibit an increase in cross section approximately 12 eV above threshold (Fig. 3), which means they go through the scattering resonance. This only occurs for the Σ states.

B. N_2

1. Branching ratios and partial cross sections

Figure 8 summarizes the measured branching ratios for photoionization of N_2 from $\hbar\omega = 17$ to 39 eV. We have only recorded the relative intensities of the three lowest energy states of the N_2 ion. These states labeled $X^2\Sigma_g^+$, $A^2\Pi_u$, and $B^2\Sigma_u^+$ have binding energies 15.6, 17.0, and 18.8 eV, respec-

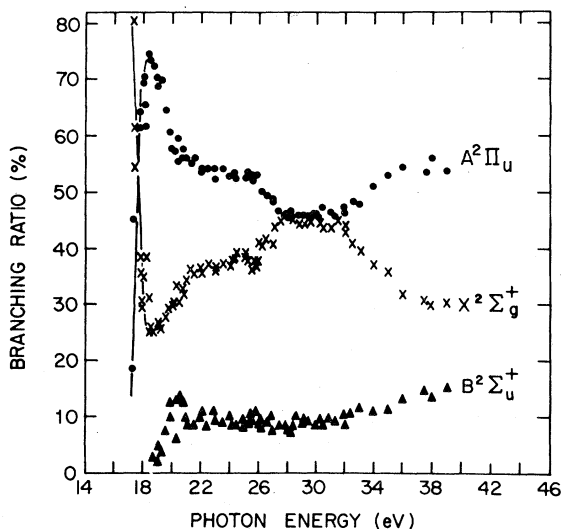


FIG. 8. Branching ratio of three states of N_2^+ as a function of photon energy.

tively. According to Hamnett *et al.*⁴⁸ the higher-binding energy states of N₂ account for ~9% of the ejected electrons at 40-eV photon energy, but only 5% at 37 eV. Therefore, our results at these high photon energies is probably 5–10% too high. The monochromator slits were usually set at 4 Å except in the region from $\hbar\omega = 17$ to 26 eV where the data were collected with 2.4-Å slits.

The partial photoionization cross sections¹⁷ (see Fig. 9) were obtained by multiplying the measured branching ratios (see Fig. 8) by the total absorption cross section,²⁰ assuming that the photoionization yield was unity.^{21,49} The data of Samson and Cairns⁵⁰ indicate that the photoionization yield for N₂ is nearly unity for higher photon energies, falling to 0.95 by $\hbar\omega = 18$ eV. The data of Wainfan *et al.*⁵¹ are in agreement with Samson and Cairns except between 21.4 and 24.8 eV where a Rydberg series converging to the C²Σ_u⁺ ionic state has been found.⁴⁵ In this wavelength region the absorption cross section increases by 10 or 15%²⁰ but the ionization efficiency may drop by an equal amount.⁵¹ A quick comparison of Figs. 8 and 9 reveals that the major contribution to the peaks in the partial photoionization cross sections near 23 eV arises from the increased absorption coefficient.²⁰ If the ionization efficiency is only 80% at 23 eV⁵¹ then much of this peak would disappear in Fig. 9. We have CIS spectra over this photon-energy range which shows the same structure as Fig. 9 except the peaks near 23 eV are reduced. Therefore, we conclude that the partial photoionization cross section, at least for the X²Σ_g⁺ and A²Π_u states, increases near 23 eV due to autoionization. The intermediate excited states of the neutral are a Rydberg series converging to the C²Σ_u⁺ state of N₂⁺ (23.6 eV).

The calculated partial photoionization cross sections for N₂ by Davenport⁷ are shown by the solid lines in Fig. 9. The peak in the X²Σ_g⁺ cross section at approximately 28-eV photon energy experimentally and at 32 eV theoretically (see Table I) is caused by the scattering resonance that we have described in the CO section. Dehmer and Dill²⁴ have shown in a calculation for K-shell photoionization of N₂ that this resonance occurs when the excited electron has approximately 11-eV kinetic energy.⁵² This final-state resonance occurs in the *l* = 3 partial wave which has σ_u symmetry. Therefore, only the 1σ_g, 2σ_g, and 3σ_g ground-state orbitals can couple to the resonance. We observe this resonance in the X²Σ_g⁺ cross section but not in the B²Σ_u⁺ cross section. It occurs at an electron kinetic energy of approximately 13 eV and has a FWHM of ~7 eV. Davenport's⁷ calculations give a peak position of 15.5 eV (kinetic energy) and FWHM of 5.5 eV. The cross sec-

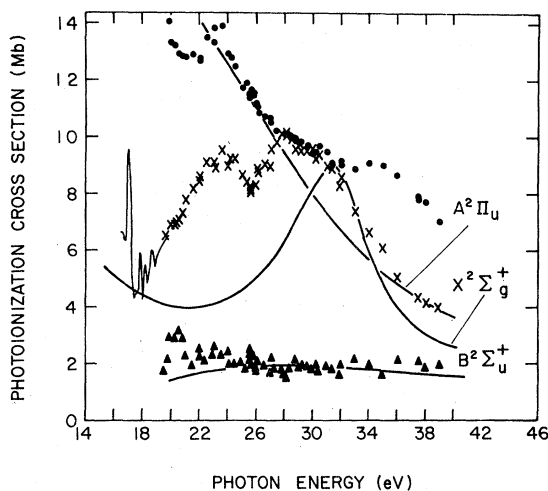


FIG. 9. Partial photoionization cross sections (Ref. 17) for the three lowest energy ionic states of N₂ as a function of photon energy. The solid curves are the calculated values from Davenport (Ref. 7). The continuation of the X²Σ_g⁺ curve below $\hbar\omega = 19$ eV represents the structure shown in Fig. 2.

tion at the peak is approximately 10 Mb from our data and 9 Mb from the calculations.⁷

The cross section for the B²Σ_u⁺ state of N₂⁺ agrees well with the calculation and shows no structure in the investigated photon-energy range except a small peak near threshold. The cross section for the A²Π_u state of N₂⁺ shows considerable deviation from the calculation between 30 and 39 eV. It would be tempting to associate this with the shape resonance, but there is no way of coupling the 1π_u initial state with a final state of appropriate symmetry. It may be that this increase in the cross section of the A²Π_u state is a result of a multiple electronic excitation similar to the series converging to the C²Σ_u⁺ state. This could be composed of Rydberg type states converging to the D²Π_g state of N₂⁺ and to the ionic state with a 2σ_g electron missing.³⁰ There is a visible increase in the absorption cross section near 440 Å (28 eV) and it appears to have a broad peak extending to 340 Å (36 eV).²⁰ It could be interesting to try to resolve line spectra in this region of the absorption spectra in an attempt to identify a possible new Rydberg series.

2. Comparison with other measurements

There are several published branching ratios for N₂⁺ at $\hbar\omega = 21.2$ eV. Our values are 36.5% for the X²Σ_g⁺ state, 55.5% for the A²Π state and 8.5% for the B²Σ_u⁺ state. The β factors have been measured for N₂,⁸ so we can correct our branching

ratios for the analyzer angular effects (Eq. 1). These corrected values are 36.5%, 53.7%, and 9.8%, respectively. The values published by Rabalais *et al.*²⁸ for 90° collection are 37, 51, and 12%, respectively, and the ratios of Blake and Carver⁴⁶ are approximately 35, 53, and 12%, respectively. Our value for the $B^2\Sigma^+$ state is lower than either of these, but in good agreement with the 8% value obtained from the electron-coincidence measurements.⁴⁸

If we extrapolate our results to 40.8 eV we obtain 30, 55, and 15%, respectively for the $X^2\Sigma_g^+$, $A^2\Pi_g$, and $B^2\Sigma_u^+$ states of N_2^+ . At this photon energy there are other ionic states which can be excited. At $\hbar\omega = 39$ eV we could not observe these states due to background effects. The results of Hamnett *et al.*⁴⁸ indicate that there is less than 10% of the signal in these states at 40 eV. In contrast Gardner and Samson³⁰ report that 22.9% of the total photoemitted current at $\hbar\omega = 40.8$ eV is associated with states of the ion with binding energy greater than 20 eV. In order to compare their results with ours, we normalized their branching ratios for the first three states of N_2^+ to 100%. The values of Gardner and Samson³⁰ are then 35.1, 53, and 11.8%, respectively. An earlier paper by Gardner and Samson⁴⁷ gave values of 31, 55.2, and 13.6%, respectively. The values reported by Rabalais *et al.*²⁸ at 40.8 eV are 28, 58.8, and 13.2%, respectively. Our extrapolated values are in reasonable agreement with all these measure-

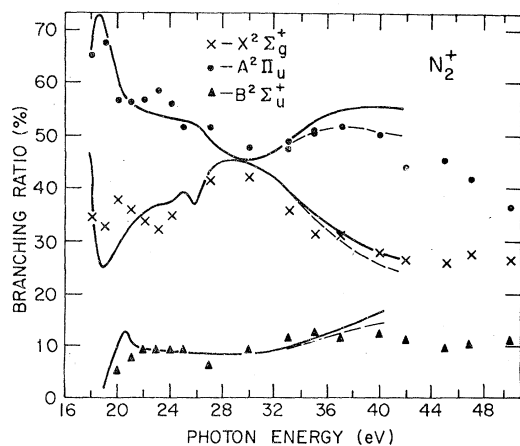


FIG. 10. Comparison of our branching ratio data for the first three states of N_2^+ with the data obtained using the high-energy inelastic electron-coincidence technique (Ref. 48). Solid curves, our data shown in Fig. 8; dashed curves, estimated changes due to the higher-energy states of N_2^+ (Ref. 48).

ments considering the magnitude of difference between different measurements.

In Fig. 10 we compare our branching ratios for the first three states of N_2^+ with those obtained using high-energy inelastic electron-coincidence scattering.⁴⁸ The solid curves represent our data, and the data points are taken from the work of Hamnett *et al.*⁴⁸ The dashed portions of the curves represent the changes in our values which would have resulted from the higher-energy states of N_2^+ observed by Hamnett *et al.*⁴⁸

The general agreement is very good with both sets of data showing the presence of the resonance in the $X^2\Sigma_g^+$ state, but not in the $B^2\Sigma_u^+$ state. Again, as in the case of CO shown in Fig. 6, the fine structure isn't present in the electron-coincidence data due presumably to the lower resolution.

3. Autoionization of N_2

The CIS curves for N_2 are shown in Fig. 2, as well as the total absorption cross section.⁵³ Table III lists all of the prominent features observed in the partial photoionization cross sections for wave lengths larger than 650 Å (<19 eV). Most of the structure in the absorption spectra of N_2 has been identified, either as Rydberg series⁵³⁻⁵⁶ or as progressions⁵⁷ of excited states. This structure appears in the partial photoionization cross sections shown in Fig. 2 due to autoionization.^{35, 58} The identification of the structure in our spectra due to autoionization is listed in Table III in terms of the identity of the excited bound states. In the wavelength range from 750 to 795 Å, autoionization is the predominant mode of photoionization and our data agree with the high-resolution photoionization study of Berkowitz and Chupka.⁵⁹ For wavelengths shorter than 750 Å, the amplitude for direct ionization becomes comparable to the amplitude of the autoionization peaks. In this region the interference between the direct photoionization and the indirect autoionization can cause distorted line shapes.³⁹ The best example of this effect is the apparent emission series⁵⁶ shown as dips in the absorption spectrum of Fig. 2 ($\lambda = 716, 690,$ and 680 Å).

There are two especially interesting autoionization features that we will discuss. The first is the vibronic autoionization seen for both the $A^2\Pi_u$ and $X^2\Sigma_g^+$ states of N_2^+ . The second is the interference effects which accompany the Hopfield⁵⁶ Rydberg series causing the apparent emission series and which are more pronounced in the cross section for the $A^2\Pi_u$ state than the $X^2\Sigma_g^+$ state. The first feature refers to the mode of coupling between the intermediate excited bound state and the final

TABLE III. Prominent features in partial photoionization cross sections of N₂.

Wavelength (Å)	Ionic state	Identification ^a
792	$X^2\Sigma_g^+$	$\left\{ \begin{array}{l} W(X^2\Sigma_g^+), m=8, v'=1 \\ R(A^2\Pi_u), m=3, v'=1 \end{array} \right.$
784	$X^2\Sigma_g^+$	$W(A^2\Pi_u), m=3, v'=3$
776	$X^2\Sigma_g^+$	$NP1, v'=0$
772	$X^2\Sigma_g^+$	$W(A^2\Pi_u), m=4, v'=1$
765 } 763 }	$X^2\Sigma_g^+$	$\left\{ \begin{array}{l} NP1, v'=1 \\ R(A^2\Pi_u), m=4, v'=2 \end{array} \right.$
758	$X^2\Sigma_g^+$	$R(A^2\Pi_u), m=5, v'=1$
754	$X^2\Sigma_g^+$	$NP1, v'=2$
748	$X^2\Sigma_g^+$	$\left\{ \begin{array}{l} W(A^2\Pi_u), m=5, v'=2 \\ R(A^2\Pi_u), m=5, v'=2 \end{array} \right.$
745	$X^2\Sigma_g^+$	$\left\{ \begin{array}{l} NP1, v'=3 \\ W(A^2\Pi_u), m=7, v'=1 \end{array} \right.$
742 ^c	$A^2\Pi_u$	Threshold $A^2\Pi_u, v'=0$
739	$X^2\Sigma_g^+, A^2\Pi_u$	$W(A^2\Pi_u), m=6, v'=2$
736	$X^2\Sigma_g^+, A^2\Pi_u$	$W(A^2\Pi_u), m=5, v'=3$
732 ^c	$A^2\Pi_u$	Threshold $A^2\Pi_u, v'=1$
730	$X^2\Sigma_g^+, A^2\Pi_u$	$R(A^2\Pi_u), m=6, v'=3$
727	$X^2\Sigma_g^+, A^2\Pi_u$	Unknown
725	$A^2\Pi_u$	Threshold $A^2\Pi_u, v'=2$
723	$X^2\Sigma_g^+, A^2\Pi_u$	$H(B^2\Sigma_u^+), m=3, v'=0$
719	$A^2\Pi_u$	$W(A^2\Pi_u), m=10, v'=3$
716 ^b	$A^2\Pi_u$	Apparent emission series
713 ^c	$A^2\Pi_u$	Threshold $A^2\Pi_u, v'=2$
709	$A^2\Pi_u$	Unknown
703	$A^2\Pi_u$	Unknown
696	$X^2\Sigma_g^+, A^2\Pi_u$	$H(B^2\Sigma_u^+), m=4, v'=0$
690 ^b	$X^2\Sigma_g^+, A^2\Pi_u$	Apparent emission series
683	$X^2\Sigma_g^+, A^2\Pi_u$	$H(B^2\Sigma_u^+), m=5, v'=0$
680	$X^2\Sigma_g^+, A^2\Pi_u$	Apparent emission series
676	$X^2\Sigma_g^+, A^2\Pi_u$	$H(B^2\Sigma_u^+), m=6, v'=0$
672	$X^2\Sigma_g^+, A^2\Pi_u$	$H(B^2\Sigma_u^+), m=7, v'=0$

^aThe identification of the Rydberg series which appear as autoionization peaks is in a shorthand notation $A(B), m, v'$; where A is a symbol for the series, B is the ionic state to which the series converges, m is the member of the series, and v' is the vibrational state of the ionic limit. $W\Pi$ is the notation for the Worley series converging to the $X^2\Sigma_g^+$ state of N_2^+ (Refs. 53–55). R is a Rydberg series converging to the $A^2\Pi_u$ state of N_2^+ (Ref. 33). H denotes Hopfield series which converges to the $B^2\Sigma_u^+$ state of N_2^+ (Ref. 53 and 54). $NP1$ refers to a new progression described by Ogawa (see Ref. 57).

^bThe apparent emission series is shown in the absorption spectra in Fig. 2. This series was first observed by Hopfield (Ref. 56).

^cThe threshold for ionization of the various vibrational levels of the $A^2\Pi_u$ state of N_2^+ are listed in the table as a reference.

state of the ion in autoionization. In general, autoionization involves configuration interaction or, simply stated, it is a two-electron process. The excited bound state of the *neutral* molecule decays to a lower-energy *ionic* state by an Auger-like process, one electron falling to a lower-energy state, another being ejected. The majority of the autoionization peaks in Fig. 2 (or Table III) are

of this type, but several are apparently due to a *different* coupling mode, vibronic. The autoionization peaks in the $A^2\Pi_u$ state of N_2^+ at $\lambda=736, 730, 719$ Å all occur due to vibronic coupling since they are associated with Rydberg series of N_2 converging to the third vibrational state of the $A^2\Pi_u$ state of the ion. The peaks at 719 and 730 Å appear to be larger in the $A^2\Pi_u$ cross section than

in the $X^2\Sigma_g^+$ cross section. This gives a way of directly comparing the two different competing autoionization channels.³⁸ Also, the peak at $\lambda = 792 \text{ \AA}$ in the partial photoionization cross section of the $X^2\Sigma_g^+$ state of N_2^+ may be due to autoionization from the eighth member of the Worley-Rydberg⁵⁸ series which converges to the first vibrational state of the $X^2\Sigma_g^+$ ionic state. This interpretation may, however, be in error as the peak is very close to threshold where measurements are difficult.

The apparent emission series seen as dips in the absorption spectra of Fig. 2 is now understood as a line shape effect due to an interference effect involving the Hopfield-Rydberg series which converges to the $B^2\Sigma_u^+$ state of N_2^+ .³⁹ This interference effect is referred to as a "window resonance." Figure 2 shows that this line shape is much more pronounced in the $A^2\Pi_u$ cross section than in the $X^2\Sigma_g^+$ cross section. There is a pronounced difference in the line shape depending upon the final state of the ion.

The increase²⁰ ($\approx 10\%$) in the photoionization cross section near 23 eV shown in Fig. 9 is a result of autoionization from Rydberg states converging to the $C^2\Sigma_u^+$ state of N_2^+ first observed by Codling.⁴⁵ He found approximately 30 lines or bands in the absorption of N_2 in the wavelength range of 484 \AA (25.6 eV) to 554 \AA (22.3 eV). Most of these lines were identified as Rydberg states converging to $C^2\Sigma_u^+$ state of N_2^+ .⁴⁵ The $C^2\Sigma_u^+$ state is obtained from the ground state of N_2 by removing one electron from the $3\sigma_g$ orbital and exciting another electron from the $1\pi_u$ orbital to the unoccupied $1\pi_g$ orbital. The Rydberg series was assumed⁴⁵ to be a $n\sigma$ type so that the one-electron configuration of the intermediate state in autoionization is $(1\sigma_g)^2(1\sigma_u)^2(2\sigma_g)^2(2\sigma_u)^2(1\pi_u)^3(3\sigma_g)^1(1\pi_g)^1(n\sigma)^1$. The total energy of this state is sufficiently large so that it could autoionize to either the $X^2\Sigma_g^+$, $A^2\Pi_u^+$, or $B^2\Sigma_u^+$ states of N_2^+ . Autoionization to either the $X^2\Sigma_g^+$ or $A^2\Pi_u^+$ state of N_2^+ would be a two electron process while autoionization to the $B^2\Sigma_u^+$ state would require three electrons to be involved. Our data shown in Fig. 9 shows that autoionization is visible in the $X^2\Sigma_g^+$ and $A^2\Pi_u$ states but not in the $B^2\Sigma_u^+$ state of N_2 .

We have already mentioned that our data probably over estimate the magnitude of increase in the photoionization cross section due to autoionization from these Rydberg states converging to the $C^2\Sigma^+$ state of N_2^+ , since the photoionization yield may decrease slightly in this region.⁵¹ There are two additional features associated with this structure which need to be pointed out. First is the nearly symmetric line shape of the autoionization at $\hbar\omega \approx 23 \text{ eV}$, both in the $X^2\Sigma_g^+$ and $A^2\Pi_u$

state of N_2^+ . This is somewhat surprising since the direct-ionization cross section is relatively large in this energy range. The potential for very asymmetrical line shapes will then exist. It is not clear why it is not actually observed. The second comment concerning this peak has to do with the "anomalous angular dependence" of the different vibrational states of the $X^2\Sigma_g^+$ state of N_2^+ observed in the energy distribution of photoelectrons at $\hbar\omega = 21.2 \text{ eV}$.⁶⁰ This behavior is undoubtedly due to the presence of these autoionization states at that particular photon energy. These angular effects are more pronounced in the $X^2\Sigma_g^+$ state than in the $A^2\Pi_u$ state because the autoionization contribution to the cross section is approximately 30% for the $X^2\Sigma_g^+$ state and only 15% for the $A^2\Pi_u$ state.

IV. SUMMARY AND CONCLUSIONS

We have presented partial photoionization cross-section data for some of the low ionization potential states of CO^+ and N_2^+ . The data are extensive enough to, for the first time, allow meaningful comparison between theory and experiment for simple molecules. Recent theoretical calculations,^{7,24} which treat the initial and final states in the photoexcitation on an equal footing, have been shown to give excellent qualitative and even good quantitative agreement with our data for the one-electron part of the spectrum.

Clearly, a semi-quantitative theoretical understanding of the many electron part of the spectrum is further away. We have identified several peaks in the photoelectron energy distributions from CO^+ as being due to shake-up peaks from a Σ state. This suggests the importance of using different photon energies for doing such identifications. It is obviously a challenging task to try to theoretically analyze the origin of these shake-ups.

We have also pointed out several interesting phenomena associated with autoionization. We have discussed the competition between different decay channels and shown that it is experimentally feasible to determine the relative importance of these. We have also shown the existence of vibronic coupling in autoionization decay for these two systems.

This work has clearly shown the advantages of synchrotron radiation for studying details of photoionization processes for molecules. A very exciting area that we have just touched is the identification of various autoionization peaks by studying the relative intensities of the various vibrational bands for a given electronic excitation.

It is also apparent that there may be interesting effects at higher photon energies. Recent photo-

ionization measurements of CO and N₂ using the *Y M*₅(132.3 eV) line show that the relative intensities of the three outer levels of CO and N₂ do not change much from 40 to 132 eV.^{61,62} For example, the relative branching ratios for the *X*, *A* and *B* states of N₂⁺ at $\hbar\omega = 132$ eV are 23, 45.3, and 31.5%⁶² compared to our values of 27, 55, and 18%, respectively. Yet the branching ratios of these three states at $\hbar\omega = 1254$ eV is 15, 7.9, and 77%. For CO the values at $\hbar\omega = 132$ eV⁶¹ ($\hbar\omega = 40$) for the same states are 16.9 (17%), 58.3(58%), and 24.7%(25%). The relative intensities of these levels at $\hbar\omega = 1254$ eV are considerably different, 25, 12, and 63%, respectively. There is a dramatic change between $\hbar\omega = 132$ eV and $\hbar\omega = 1254$ eV.

ACKNOWLEDGMENTS

We would like to thank Dr. J. W. Davenport, Dr. J. L. Dehmer, and Dr. D. L. Ederer for discussions and comments on the manuscript. It is also a pleasure to thank the staff at the synchrotron radiation center, particularly E. M. Rowe and R. Otte, for their cooperation and support.

APPENDIX

The flux from the 1-m Seya-Namioka monochromator is shown in Fig. 10, where the curve is plotted per 1-Å slits and 1 mA of beam current. There are two curves shown in Fig. 11, the lower amplitude curve represents the flux throughout most of this experiment. The larger amplitude curve is the flux after the mirror in the beam line had been replated and the grating in the monochromator replaced. The data for CO above 40-eV

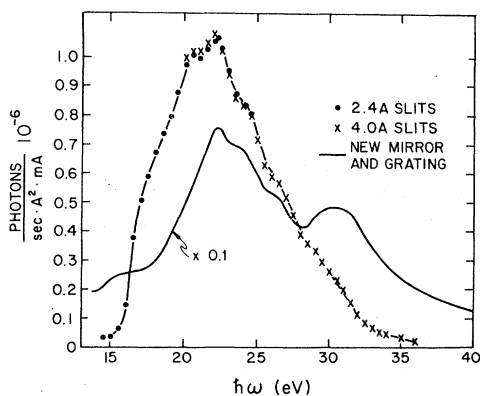


FIG. 11. The measured number of photons per sec per mA of beam current as a function of photon energy. The measurements were made using a NBS calibrated photodiode (Ref. 11) for two values of slit settings and normalized to 1-Å slits. The solid curve is the flux after the mirror in the beam line was replated and the grating replaced.

photon energy were taken after these changes were made. It is obvious that the characteristics of the optical system can be much more important in determining counting rates than the properties of the storage ring *per se*.

The transmission of the energy analyzer must be known in order to obtain branching ratios from an electron kinetic energy distribution. The energy analyzer can be run in either of two modes. At low pass energy (high resolution) the volume the analyzer can accept (V_A) will be smaller than the source region (V_S) (the source region is the region of intersection of the gas beam and the light). The acceptance volume is then determined by the kinetic energy of the photoelectrons, being larger for small kinetic energies. This accentuates the low-energy electrons. At high pass energies (low resolution), on the other hand, $V_A > V_S$. The sampled volume is then constant independent of the kinetic energy of the electrons. As we are interested in branching ratios, we obviously wish to perform our measurements in this mode. This can be tested by measuring the ratio of the intensities of two peaks in the photoelectron spectra at a fixed photon energy as a function of the pass energy of the analyzer. Above a sufficiently high pass energy the ratios should not change, indicating that the acceptance volume of the analyzer has exceeded the source size.

Figure 12 shows the normalized intensity ratios for three peaks in the photoelectron spectra of CO (see Fig. 1) at $\hbar\omega = 21.2$ eV, as a function of pass energy. The *x*'s represent the ratio of the area of the $X^2\Sigma^+$ state (binding energy 14 eV) to the $B^2\Sigma^+$ state (binding energy 19.7 eV), the *o*'s

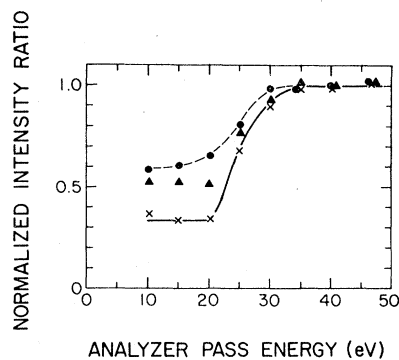


FIG. 12. Ratios of the integrated signals from the $B^2\Sigma^+$, $A^2\Pi$, and $X^2\Sigma^+$ states of CO⁺ at 21.2 eV. The kinetic energy of the electrons from these states is approximately 1.5, 4.2, and 7.2 eV, respectively. The *x*'s are the normalized ratio of the $X^2\Sigma^+$ state to the $B^2\Sigma^+$ state (normalization 2.61). The *▲*'s are the ratio of the $A^2\Pi$ state to the $B^2\Sigma^+$ state (normalization 5.09). The *●*'s are the ratio of the $X^2\Sigma^+$ state to the $A^2\Pi$ state (normalization 0.51).

are the ratios of the $A^2\Pi$ state (binding energy ~ 17 eV) to the $X^2\Sigma^+$ state, and the Δ 's are the points for the ratio of the $A^2\Pi$ state with respect to the $B^2\Sigma^+$ state. These ratios have all been normalized to the average values obtained for many runs at a pass energy of 40 eV (see figure caption). For this photon energy the normalized ratios are independent of pass energy above 30 eV. There is also a smooth transition regime where $V_A < V_S$ for one or two of the ionic states but not

for all three of them. The normalized ratio becomes a constant for each state at sufficiently low pass energy, since we are then in the regime where the acceptance volume for each state is determined by its kinetic energy. The experimentally observed ratio in this region of pass energy indicates that the analyzer system distorts the amplitude of the spectra by a factor which is the ratio of the kinetic energies to the $3/4$ power.

*The University of Wisconsin Physical Sciences Laboratory Synchrotron Center is supported by NSF Grant No. 74-15098.

†Research supported by the Laboratory for Research on the Structure of Matter and the Advanced Research Projects Agency of the Department of Defense as monitored by the Air Force Office of Scientific Research under contract No. F44620-75-C-0069 and the NSF under grants DMR 2-0325 and 73-07682.

‡Present address: Deutsches Elektronen-Synchrotron DESY, Hamburg, Germany.

¹J. A. R. Samson and J. L. Gardner, *J. Electron Spectrosc.* **8**, 35 (1976).

²T. Gustafsson, E. W. Plummer, D. E. Eastman, and J. L. Freeouf, *Solid State Commun.* **17**, 371 (1975).

³E. W. Plummer, *Topics in Applied Physics*, edited by R. Gomer (Springer-Verlag, Berlin, 1975) Vol. 4, p. 143; *The Physical Basis for Heterogeneous Catalysis*, edited by E. Drauglis and R. I. Jaffee (Plenum, New York, 1975), p. 203.

⁴J. E. Demuth and D. E. Eastman, *Phys. Rev. Lett.* **32**, 1123 (1974).

⁵E. W. Plummer, B. J. Waclawski, and T. Vorburger, *Chem. Phys. Lett.* **28**, 510 (1974).

⁶At present we have measured approximately 10 different molecules.

⁷J. W. Davenport, *Phys. Rev. Lett.* **36**, 945 (1976).

⁸T. A. Carlson, G. E. McGuire, A. E. Jonas, K. L. Cheng, C. P. Anderson, C. C. Lu, and B. P. Pullen, *Electron Spectroscopy*, edited by D. A. Shirley (North-Holland, Amsterdam, 1972), p. 207.

⁹E. M. Rowe and F. E. Mills, *Part. Accel.* **4**, 211 (1973).

¹⁰D. E. Eastman, D. W. Grobman, J. L. Freeouf, and M. Erbudak, *Phys. Rev. B* **9**, 3472 (1974).

¹¹A NBS calibrated windowless Al_2O_3 photodiode (No. 93) was used to measure the photon flux. L. R. Canfield, R. G. Johnston, and R. P. Madden, *Appl. Opt.* **12**, 1611 (1973).

¹²The polarization is estimated to be 80%.

¹³PHI model No. 250.

¹⁴The pressure above the nozzle was estimated by moving the nozzle out of position, and observing the change in counting rates.

¹⁵C. N. Yang, *Phys. Rev.* **74**, 764 (1948).

¹⁶G. J. Lapeyre, J. Anderson, P. L. Gobby, and J. A. Knapp, *Phys. Rev. Lett.* **33**, 1290 (1974).

¹⁷The cross section contains the angular dependence given by Eq. (1).

¹⁸W. Gudat and D. E. Eastman (unpublished).

¹⁹The gold foil is being calibrated against the Al_2O_3 diode.

²⁰L. C. Lee, R. W. Carlson, D. L. Judge, and M. Ogawa, *J. Quant. Spectrosc. Radiat. Transfer* **13**, 1023 (1973).

²¹G. R. Wight, M. J. Van der Wiel, and C. E. Brion, *J. Phys. B* **9**, 675 (1976).

²²K. Codling and A. W. Potts, *J. Phys. B* **7**, 163 (1974).

²³M. Sasanuma *et al.*, *Third International Conference Vacuum Ultraviolet Radiation Physics*, edited by Y. Nakai (Physical Society of Japan, Tokyo, 1971).

²⁴J. L. Dehmer and D. Dill, *Phys. Rev. Lett.* **35**, 213 (1975).

²⁵J. W. Davenport, Ph.D. thesis (University of Pennsylvania, 1976) (unpublished).

²⁶The peak in the $2\Sigma^+(3\sigma)$ is not clearly resolved in our spectra, because of the limited photon-energy range. Our numbers for the photon energy of the peak position in the cross section could easily be a volt low.

²⁷C. L. Allyn, T. Gustafsson, and E. W. Plummer, *Chem. Phys. Lett.* (to be published).

²⁸J. W. Rabalais, T. P. Debies, J. L. Berkosky, J.-T. J. Huang, and F. O. Ellison, *J. Chem. Phys.* **61**, 516 (1974).

²⁹J. L. Bahr, A. J. Blake, J. H. Carver, J. L. Gardner, and V. Kumar, *J. Quant. Spectrosc. Radiat. Transfer* **12**, 59 (1972).

³⁰J. L. Gardner and J. A. R. Samson, *J. Chem. Phys.* **62**, 1447 (1975).

³¹K. Siegbahn *et al.*, *ESCA Applied to Free Molecules* (North-Holland, Amsterdam, 1969).

³²A. W. Potts and T. A. Williams, *J. Electron Spectrosc.* **3**, 3 (1974).

³³M. J. Van der Wiel and C. E. Brion, *J. Electron Spectrosc.* **1**, 309 (1972), see also A. Hammett, W. Stoll, and C. E. Brion, *ibid.* **8**, 367 (1976).

³⁴C. Backx, K. Klewer, and M. J. Van der Wiel, *Chem. Phys. Lett.* **20**, 100 (1973).

³⁵Th. M. El-Sherbini and M. J. Van der Wiel, *Physica* **59**, 433 (1972).

³⁶L. C. Lee, R. W. Carlson, and D. L. Judge, *J. Phys. B* **9**, 855 (1976).

³⁷(a) L. C. Lee, R. W. Carlson, D. L. Judge, and M. Ogawa, *J. Geophys. Res.* **79**, 5286 (1974); (b) L. C. Lee (private communication).

³⁸C. Duzy and R. S. Berry, *J. Chem. Phys.* (to be published).

³⁹U. Fano, *Phys. Rev.* **124**, 1866 (1961).

⁴⁰R. E. Huffman, J. C. Larrabee, and Y. Tanaka, *J. Chem. Phys.* **40**, 2261 (1964).

⁴¹C. R. Cook, P. H. Metzger, and M. Ogawa, *Can. J.*

- Phys. 43, 1706 (1965).
- ⁴²Y. Tanaka, Sci. Paper Instrum. Phys. Chem. Research (Tokyo) 39, 447 (1942).
- ⁴³M. Ogawa, J. Chem. Phys. 43, 2143 (1965).
- ⁴⁴T. Gustafsson, E. W. Plummer, W. Gudat, and D. E. Eastman (unpublished).
- ⁴⁵K. Codling, Astrophys. J. 143, 552 (1966).
- ⁴⁶A. J. Blake and J. N. Carver, J. Chem. Phys. 47, 1038 (1967).
- ⁴⁷J. L. Gardner and J. A. R. Samson, J. Electron Spectrosc. 2, 259 (1973).
- ⁴⁸Hamnett, Stoll, and Brion, Ref. 33.
- ⁴⁹R. D. Hudson, Natl. Stand. Ref. Data Ser., Nat. Bur. Stand. 38 (1971).
- ⁵⁰J. A. R. Samson and R. G. Cairns, J. Geophys. Res. 69, 4583 (1964); J. Opt. Soc. Am. 55, 1035 (1965).
- ⁵¹N. Wainfan, W. C. Walker, and G. L. Weessler, Phys. Rev. 99, 542 (1955).
- ⁵²The widths and position of the calculated resonance depends upon the value of α , i.e., the coefficient for the Slater ($\rho^{1/3}$) approximation for exchange and correlation. Davenport's values are for $\alpha=0.751$, while Dehmer and Dill used $\alpha=1$ (Ref. 24).
- ⁵³R. E. Huffman, Y. Tanaka, and J. C. Larrabee, J. Chem. Phys. 39, 910 (1963).
- ⁵⁴R. E. Worley, Phys. Rev. 64, 207 (1943); 89, 863 (1953).
- ⁵⁵M. Ogawa and Y. Tanaka, Can. J. Phys. 40, 1593 (1962).
- ⁵⁶J. J. Hopfield, Phys. Rev. 36, 789 (1930).
- ⁵⁷M. Ogawa, Can. J. Phys. 42, 1087 (1964).
- ⁵⁸The curves in Fig. 2 are proportional to the partial-photoionization cross section and inversely proportional to the photoyield of Au. They do not depend upon the photoionization yield.
- ⁵⁹J. Berkowitz and W. A. Chupka, J. Chem. Phys. 51, 2341 (1969).
- ⁶⁰T. A. Carlson and A. E. Jonas, J. Chem. Phys. 55, 4913 (1971).
- ⁶¹M. S. Banna and D. A. Shirley, J. Electron Spectrosc. (to be published).
- ⁶²R. Nilsson *et al.*, Uppsala University Report, UIIP-912, 1975 (unpublished).